

DESIGN, CONTROL AND EVALUATION OF A WHOLE-SENSITIVE ROBOT ARM FOR PHYSICAL HUMAN-ROBOT INTERACTION

DZMITRY TSETSERUKOU* and NAOKI KAWAKAMI†

*Department of Information Physics and Computing,
the University of Tokyo, 7-3-1 Hongo,
Bunkyo-ku, Tokyo, 113-8656, Japan*

**dima_teterukov@ipc.i.u-tokyo.ac.jp*

†Naoki_Kawakami@ipc.i.u-tokyo.ac.jp

SUSUMU TACHI

*Graduate School of Media Design, Keio University,
4-1-1 Hiyoshi, Kohoku-ku, Yokohama, 223-8526, Japan
tachi@tachilab.org*

Received 9 June 2008

Accepted 4 July 2009

The paper focuses on design and control of a new anthropomorphic robot arm enabling the torque measurement in each joint to ensure safety while performing tasks of physical interaction with human and environment. When the contact of the robot arm with an object occurs, local admittance algorithm provides active compliance of corresponding robot arm joint. Thus, the whole structure of the manipulator can safely interact with an unstructured environment. The detailed design procedure of the 4-DOF robot arm and optical torque sensors is described in the paper. The experimental results of joint admittance control revealed the feasibility of the proposed approach to provide safe interaction of entire structure of robot arm with a person. The control system with load angle position feedback and lead compensator is proposed to improve dynamic behavior of flexible joint arm. The experimental results show high performance of the developed controller in terms of successful damping of vibrations.

Keywords: Human-robot physical interaction; robot arm; optical torque sensor; admittance control.

1. Introduction

In near future, robots will be introduced in human daily life environment to assist with hospital care, surgery operations, high-risk maintenance tasks, construction works, and office affairs. The desired coexistence of robotic systems and humans in the same physical domain (sharing the same workspace and actually cooperating in a physical manner) poses very fundamental problem of ensuring safety to the user and robot. Even without wrong programming, a robot, moving freely in a human

environment, is potentially dangerous because of its large moving masses, powerful actuators and unpredictably complex behavior. A robot falling on someone or just stepping on his foot by mistake might cause much more damage to the victim than a human being of the same size. Thus, following the First Law of robotics introduced by I. Asimov¹ in 1942: “A robot may not injure a human being, or, through inaction, allow a human being to come to harm” — is the key aspect for successful integration of robots into human environment. Design and programming of the robots exhibiting intrinsically safe behavior in a human domain are great challenges in robotics because such robots have to deal with unstructured time-varying environment. Several humanoid robots aimed at integration into people environment were developed. The Honda’s ASIMO² and HRP 2³ show the best performance among humanoid robots while cooperating with human being. However, despite the splendid means for sensing the environment (visual, audio, and a sense of touch), the 6 axis force/torque sensors attached at the tip of the robot arm and a stereo vision system which is slow to track the changing environment in real-time, are only the abilities to anticipate the collision. The rest parts of the robot body (forearm, elbow, upper arm, shoulder, and torso) are presenting the significant danger not only for human being, but also for the robot structure itself.

Several effective methods for enhancement of contact detection ability of manipulator were reported. To avoid collisions in time-varying environment, Lumelsky *et al.*⁴ proposed to cover a manipulator with a sensitive skin capable of detecting nearby objects. Mitsunaga *et al.*⁵ progressively improved the tactile ability of the robot through covering its entire body with piezoelectric film-based tactile sensors. Since this device integrates a huge amount of small sensors incorporated into soft layer, and requires complicated wiring and signal processing hardware, it has high cost and reliability issues. Finding the technical solution for trade-off between performance and safety is the target of a new manipulation technology. To cope with this issue, an active compliance control implying the fast joint torque controlling based on measuring the applied external torque in each joint was developed. The first embodiment of torque measurement is the integration of a torque sensor into each joint of the manipulator. The impedance control generates compliant trajectory based on information on the measured external torque. Such approach has two main advantages: (1) sensor detects not only forces applied to the robot hand but also those exerted at other points on the manipulator, (2) and allows to increase the performance of fast movements by active vibration damping. Several attempts have been made by researchers to improve the joint torque control. Wu and Paul⁶ proposed a simple, wide bandwidth, torque servo system using strain-gauge-based joint torque sensor. The torque-controlled lightweight robot arm with high load to weight ratio was developed by Hirzinger *et al.*⁷ Each joint of the arm is facilitated with strain-gauge-based torque sensor, position sensor and piezzo-brake. Sakaki and Iwakane⁸ proposed to use a compact motor drive with embedded magnetostrictive torque sensor for impedance control of the robot arm. The approach of torque measurement through the elasticity of the harmonic drive flexsplines allows keeping the

same stiffness and mechanical structure of the robot.^{9,10} This method requires the strain gauges to be installed on the flexsplines. The crucial shortcomings of the torque measurement approaches mentioned above will be discussed in Sec. 3.

The alternative method for increasing the safety level of robot arms interacting with humans is the intentionally introducing the compliance at the mechanical design level. The main idea here is the decoupling the rotor inertia from the link inertia through use of passive elasticity.¹¹ However, the robot control is complicated by many unknown parameters (e.g., actuator stiffness and damping). Furthermore, compliant transmission negatively affects the performance in term of increased oscillations and settling time.

Our main research is devoted to realization of teleoperated robot enabling safe interaction with humans. The line of master-slave robot systems (TELESAR I and TELESAR II) was successfully developed in our laboratory.^{12,13} The performance and stability of teleoperation were gradually improved. The slave robot enables to perform dexterous operations by means of 7-DOF arms and 8-DOF hands. The safety in interaction at the tip of the end-effector is provided by impedance control algorithm.

To realize the safe physical contact of entire robot arm structure with human, our primary idea is concentrated on the design of a whole-sensitive robot arm (by using distributed torque sensors in each joint). When contact with environment occurs, manipulator automatically generates compliant motion according to the measured external torque and time derivative of torque. The developed anthropomorphic manipulator iSoRA (**i**ntelligent **S**oft **R**obot **A**rm) having 4-DOF arm and 8-DOF hand (Fig. 1) is capable of safe physical interaction with environment wherever contact occurs on the arm surface. The distinctive features of our approach are as follows:

- (1) We use an optical approach to the torque measurement, which allows avoiding inherent shortcomings of strain-gauge-based and magnetostrictive force/torque sensors. The developed new optical torque sensors have high dependability, good accuracy (even in electrically noisy environment), low price, compact sizes, and easy manufacturing and calibration procedure.¹⁴
- (2) The stiffness of the sensor developed by us is much smaller than in previously proposed sensors. So, when the collision takes place, the injuries of human can be considerably reduced through compliant coupling between the motor rotor inertia and the link inertia.
- (3) The admittance control was employed to realize safe and smooth human-robot interaction and to provide the effectiveness of the contact task performance.

The teleoperated robot arm is controlled by the operator's motion (Fig. 2). To achieve human-level dexterity of manipulation, the master arm was endowed with 6 DOF (Fig. 3). The motion of the operator's elbow is controlled by the accelerometer-based position sensor. In order to make the level of motion constraint lower, the



Fig. 2. Operator cockpit.



Fig. 3. Masterarm.

↔
Position
Orientation
Velocity

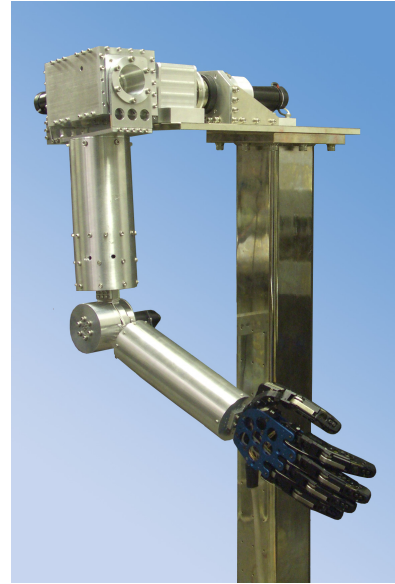


Fig. 1. Developed whole-sensitive robot arm.

manipulator was manufactured using components with small inertia and embedded gravity compensation mechanism. During operation of manipulator the movement information (position, orientation and velocity) is acquired through motor encoders installed into each joint of the master arm.

The remainder of the paper is structured as follows. Section 2 describes the development of a whole-sensitive robot arm. Newly developed optical torque sensors are presented in Sec. 3. The admittance control algorithm allowing compliant interaction with environment, effect of joint flexibility on robot arm dynamics, and the experimental results are discussed in Sec. 4. In Sec. 5, we conclude the paper.

2. Design of a New Anthropomorphic Robot Arm

From the safety point of view, to minimize injuries in the case of collision, most of the robot arm parts were manufactured from aluminium alloys to obtain as much lightweight structure as possible. The robot links were designed in round shape to reduce impact force. The distribution of the arm joints replicates the human arm structure in order to make it easier to operate using kinesthetic sensation during teleoperation.

To remove mechanical subsystems without disassembling the main structure when the failures do occur, we use a modular approach while designing the anthropomorphic robot arm. Therefore, we selected CSF-series gear head type of harmonic drive instead of compact and lightweight component one. The harmonic drive offers such advantages as accurate positioning, high torque capability, torsional stiffness,

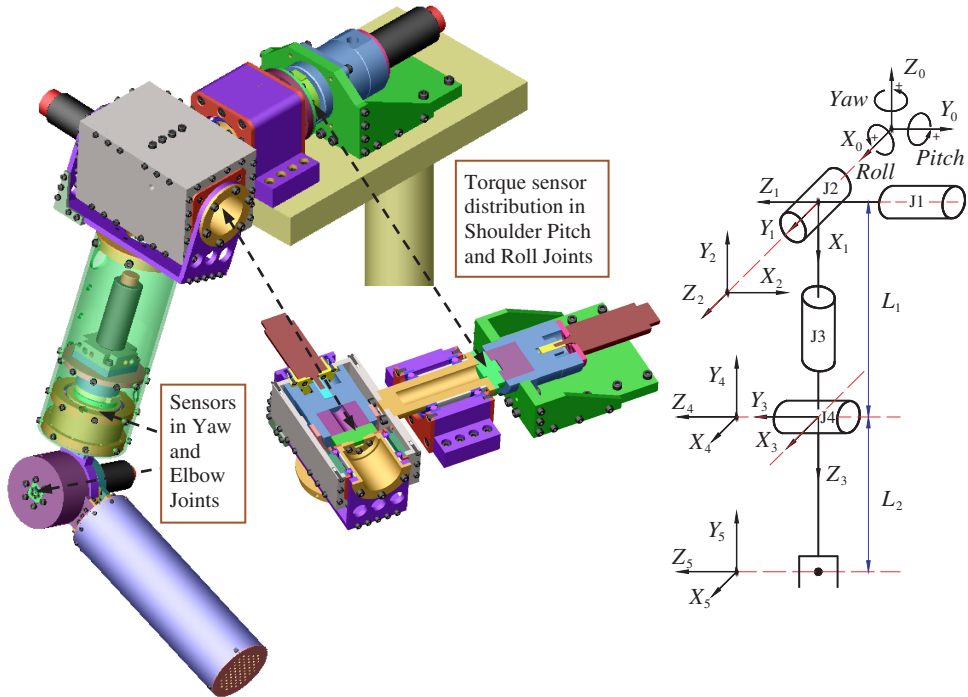


Fig. 4. 3D CAD arm model and coordinate systems.

and high single stage ratios. Developed robot arm iSoRA has 4-DOF: roll, pitch, yaw joints of a shoulder, and a pitch joint of an elbow. Such orthogonal disposition of the axes simplifies the installation of the torque sensors and motor drives into the joints, allowing thus avoidance of application of additional belt driven actuators. The 3D CAD model of the developed arm and coordinate systems based on Denavit-Hartenberg convention are represented in Fig. 4.

Each robot joint is equipped with optical torque sensor directly connected to the output shaft of harmonic drive. The sizes and appearance of the arm were chosen so that any sense of incongruity during interaction with a human is avoided. We kept the arm proportions the same as in average height Japanese male, aged 25: upper arm length L_1 0.308 m; upper arm circumference 0.251 m (diameter 0.080 m); forearm length L_2 0.241 m; forearm circumference 0.189 m (diameter 0.06 m). The motors are equipped with magnetic encoders having 512 pulses per revolution. To protect the sensor against influence of bending moment and axial force, the simple supported loaded shaft configuration was implemented using two sets of bearings. The kinematic parameter values are listed in Table 1.

To calculate the motor power, we considered cyclical movement of drive in accordance with the torque-speed diagram. The movement cycle time of 1.2 sec with angular speed of $\pi/2$ rad/sec was assumed. The acceleration period of 25% of the

Table 1. Denavit-Hartenberg parameters of the arm.

i	α_{i-1} [deg]	a_{i-1} [m]	d_i [m]	θ_i [deg]
1	90	0	0	$\theta_1 - 90$
2	-90	0	0	$\theta_2 + 90$
3	90	0	L_1	$\theta_3 + 90$
4	-90	0	0	$\theta_4 - 90$
5	0	L_2	0	0

Table 2. Principal specifications.

Parameters	Arm joints			
	Shoulder			Elbow
	J1, Pitch	J2, Roll	J3, Yaw	J4, Pitch
Mobility range (New robot arm/ Human arm) [deg]	-180 to 180 (-60 to 180)	-180 to 10 (-165 to 0)	-180 to 180 (-60 to 180)	0 to 112 (0 to 130)
Motor power[W], motor type	90.0, Maxon RE 35	60.0, Maxon RE 35	26.6, Faulhaber 2657	26.6, Faulhaber 2657
Harmonic drive rated torque [Nm], (type/gear ratio)	7.8, (CSF-14-GH /100)	7.8, (CSF-14-GH /100)	5.0, (CSF-11- 2XH/100)	5.0, (CSF-11- 2XH/100)

positioning time and standstill time of 0.2 sec were defined. The root mean squared values of required torque of the entire work cycle were calculated for the motors of each joint using preliminary information of moment of inertia of the motor rotor, moment of inertia of the load, angular acceleration, the efficiency of harmonic drives, the load torques, and friction torques. To provide high output torque of drive and small sizes of the motor side, the harmonic drive with high gear ratio of 100 was adopted.

The principal specifications of the developed arm are given in Table 2.

3. Development of a New Optical Torque Sensor

Strain gauges are widely used to measure the exerted force value providing such benefits as high linearity, about 0.03%–2.5% of full scale (FS), and high resolution. However, their maximum allowable strain is close to their breaking point. To guarantee overload protection of transducers, mechanical stops with very small clearances limiting deflections of flexures are necessary. Moreover, such sensors have considerable electrical noise level, fragility, complicated manufacturing procedure, etc. Furthermore, in case of noisy environment (e.g., in close vicinity of powerful DC motor creating high level of electromagnetic noise), the additional low-pass filter reducing bandwidth of the signal to as small as 10–20 Hz is required to get readable data.

In order to facilitate the realization of local impedance control in each robot arm joint, we developed new optical torque sensors having high reliability, high accuracy (even in electrically noisy environment), easy mounting procedure, and low price.

In our previous work, we described the techniques of the torque measurement, their advantages and shortcomings, and pointed out the motivations behind using an optical approach.¹⁴ Hirose and Yoneda¹⁵ proposed to use a split type photodiode to detect the 2D displacement of light source (LED) caused by the applied force. In cooperation with Minebea Co., OPFT series of 6-axes optical force sensors were manufactured.^{16,17} In comparison with conventional transducers, they have electrical noise immunity and low cost. However, these sensors suffer from complicated calibration procedure, and have an average accuracy of 5% FS. The list of desirable properties of torque sensor aimed at anthropomorphic robot arm integration is given as follows:

- (1) Addition of the torque sensor to a robot joint should cause a minimal modification in kinematics and dynamics. Therefore, lightweight sensor with small width is preferable.
- (2) High signal-to-noise ratio ensuring a high resolution of the torque measurement is desirable.
- (3) Torsional stiffness of the sensor should not considerably reduce the natural frequency of the robot arm.
- (4) Mechanical structure should be machined from a single piece of metal in order to eliminate hysteresis.
- (5) Influence from the non-torsional components of the load should be avoided.
- (6) Simple to manufacture, low in cost, and robust.

The novelty of our method is the application of the ultra-small-size photointerrupter (PI) RPI-121 as a sensitive element to measure the relative motion of sensor components. The linear section of the transferring characteristic corresponding approximately to 0.2 mm can be used for detection of the relative displacement of the object.¹⁸ The dimensions of the PI (RPI-121: 3.6 mm × 2.6 mm × 3.3 mm) and its weight of 0.05 g allow realization of compact design. Furthermore, PI also has small influence from the electromagnetic field and stray light. Separation of the sensing element from the deflected beams results in high robustness of the sensor. We developed several sensor prototypes with cross-shaped, hub-spoke-shaped, ring-shaped, and semi-circular-shaped flexure on the basis of FEM analysis results in order to find out the optimal solution. Because of sufficient stiffness, high natural frequency and small influence of bending moment and axial force on the sensor accuracy, the spoke-shaped spring as deflecting part of the optical torque sensor was chosen. The optical torque sensor is set between the driving shaft of the harmonic transmission and driven shaft of the joint (Fig. 5).

When the load is applied to the arm, the spring in corresponding joints is deflected. This causes the adapter plate rotation with small angle of twist, θ . The shield displacement is detected by the degree of interruption of infrared light that

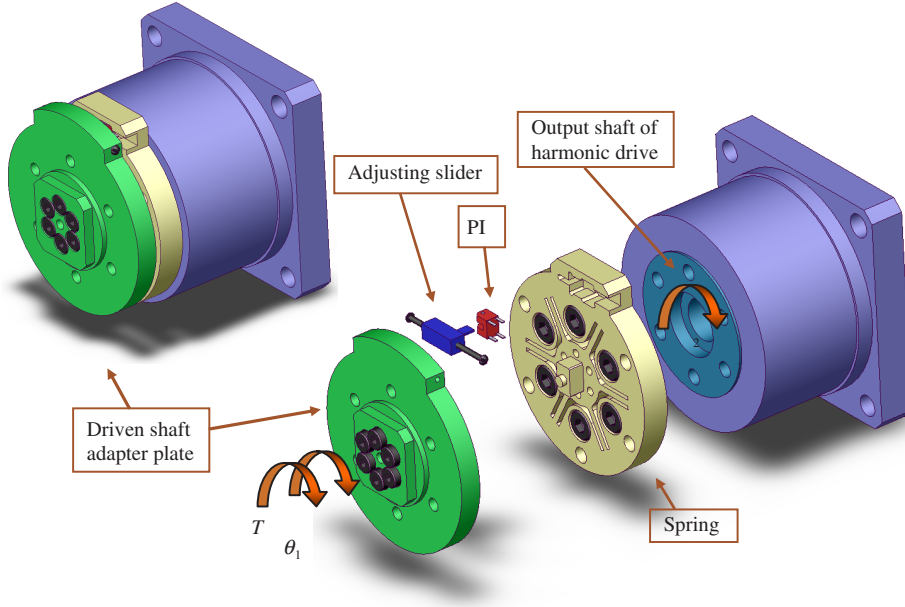


Fig. 5. 3D model of the optical torque sensor aimed at robot arm application.

falls on the phototransistor. Thus, the magnitude of the output signal from PI corresponds to the exerted load. The relationship between the sensed torque, T , and the angle of twist is the following:

$$T = k\theta = k(\theta_1 - \theta_2), \quad (1)$$

where k is the torsional stiffness of the spring member.

Since the angle of twist is small, it can be calculated from the displacement of the shield in the tangential direction, Δx :

$$T = k\Delta x/R, \quad (2)$$

where R is the distance from the sensor center to the middle axis of the shield plate in radial direction.

The drawing of the hub-spoke-shaped spring is presented in Fig. 6.

The detector consists of an inner part 1 connected by flexure 3 with an outer part 2, a fixed PI 5, and a shield plate 4. A protrusion 6 is intended for axial alignment of a spring with an output shaft of harmonic drive. A part 7 is provided for increasing the transferring torque rate and diminishing hysteresis. The zero position of a shield is adjusted by rotation of screw while sensor assembling. The torsional stiffness¹⁹ of the sensor is derived from:

$$k = 4NEI \left(\frac{1}{l} + \frac{3r}{l^2} + \frac{3r^2}{l^3} \right), \quad (3)$$

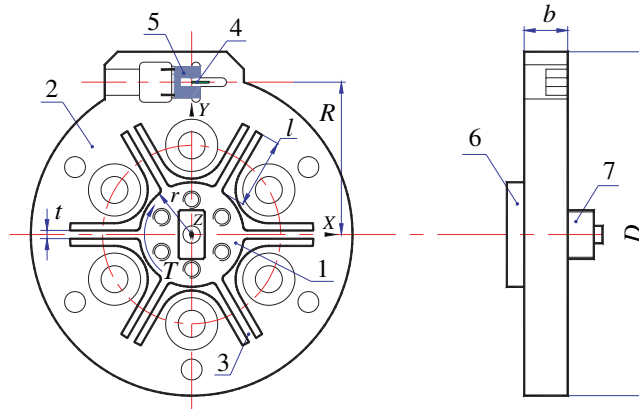


Fig. 6. Hub-spoke structure layout.

where N is the number of spokes; E is the modulus of elasticity, I is the moment of inertia of the spoke cross section, l is the spoke length, and r is inner radius of the sensor.

The value of I can be calculated as follows:

$$I = bt^3/12, \quad (4)$$

where b is the beam width, t is the beam thickness (Fig. 6).

The sensing range of sensors was calculated using gravity force value and contact force of ± 25 N at the tip of the robot arm. The sensors attached to the first, second, and third/fourth joints were designed to measure torque of ± 12.5 Nm, ± 10.5 Nm, and ± 4.5 Nm, respectively. Such materials as high yield-strength stainless steel 17-4PH, 13-8 VAR as well as AISI 4135 and 4130 steel can be used for manufacturing the spring member. We decided to use AISI 4135 steel with tensile yield strength σ_{yield} of 785 MPa. The results of analysis of third/fourth joint sensor using FEM demonstrate von Mises stress $\sigma_{VonMises}(T_z)$ in MPa under a torque T_z of 4.5 Nm (Fig. 7(a)), tangential displacement in mm (Fig. 7(b)), stress under a bending moment T_x of 4.5 Nm (Fig. 7(c)), and stress under an axial force F_z of 70 N (Fig. 7(d)).

The results of analysis show that spring also has sufficient strength to support bending and axial load. The torsional stiffness is calculated from Eq. (2) using tangential displacement (Fig. 7(a)). The spring components were manufactured from one piece of AISI 4135 steel using a wire electrical discharge machining (EDM). Components and assembly of the torque sensor incorporated in second joint are presented in Fig. 8.

The test rig for calibration of the optical sensor was developed (Fig. 9(a)). Loading torque was created by means of attachment of reference weights to the lever arm. Calibration results for torque sensor attached to elbow joint are presented in Fig. 9(b).

708 *D. Tsetserukou, N. Kawakami & S. Tachi*

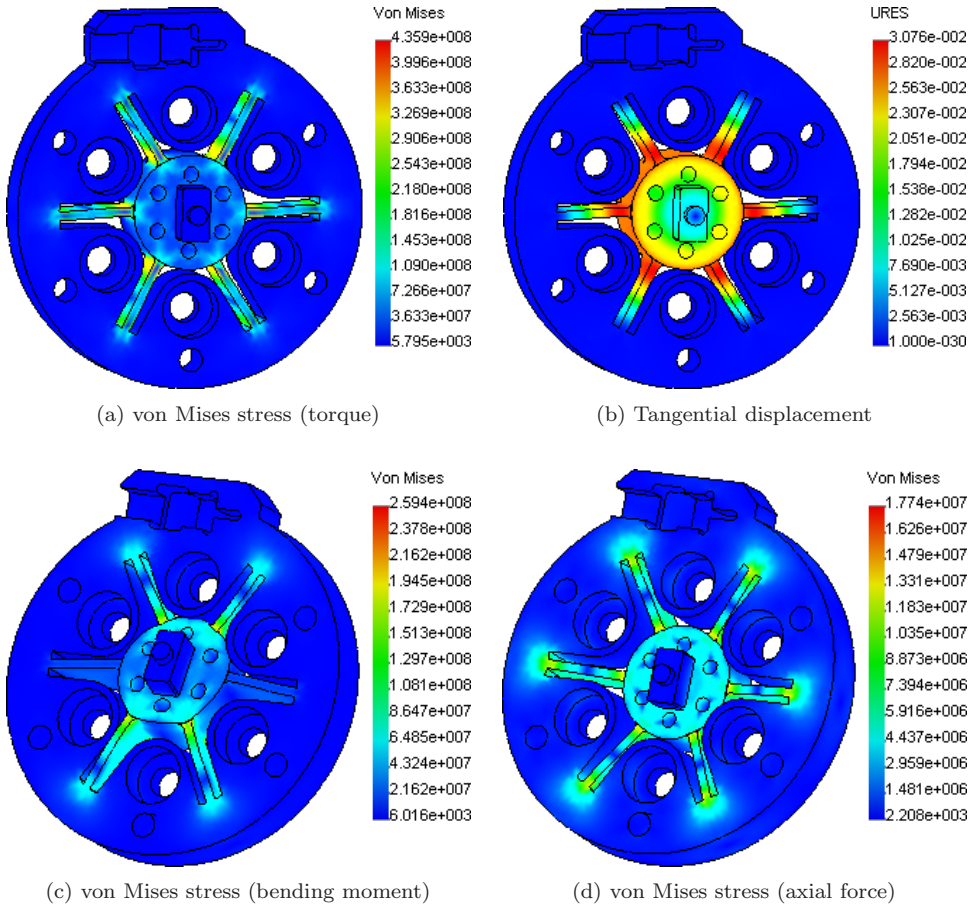


Fig. 7. Results of FEM analysis of sensor in the third/fourth joints.

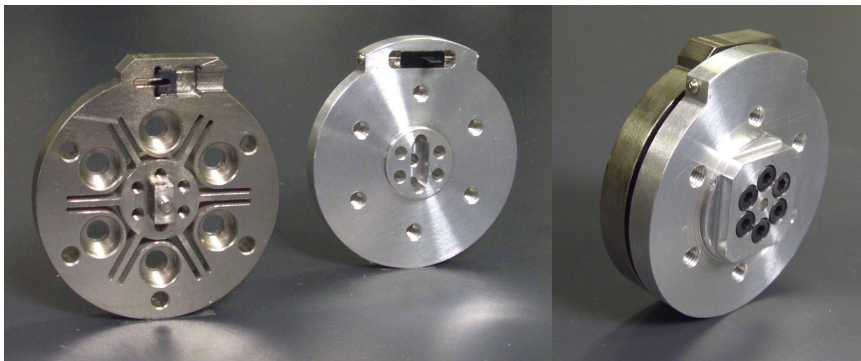


Fig. 8. Torque sensor of shoulder pitch joint.

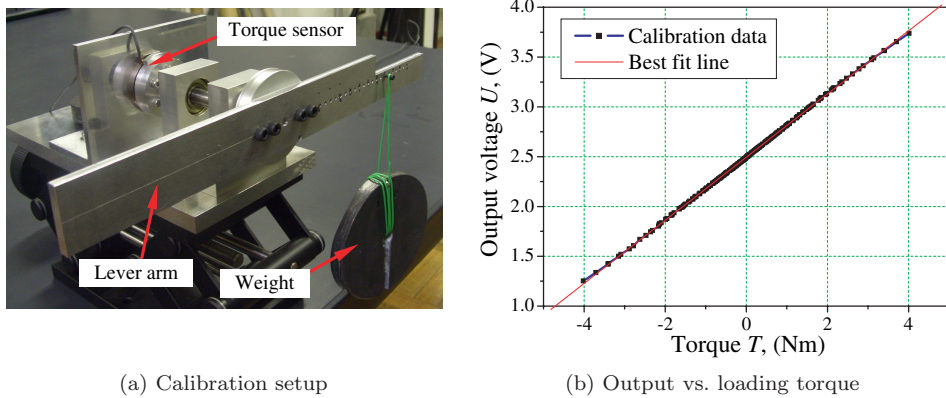


Fig. 9. Calibration setup and calibration results.

In order to determine the sensitivity and non-linearity of the optical torque sensors, we used the best-fit line approach. Calculated sensitivity of the transducer attached to the fourth joint equals 0.317 V/Nm . Non-linearity of 2.5% of Full Scale was calculated using maximum deviated value from the best-fit line. Torque sensor resolution was determined based on the least significant bit value and calibration diagram. For the torque sensors attached to the first, second, and third/fourth joints, resolution equals 10.77 mNm , 9.02 mNm , and 4.31 mNm , respectively. The average signal-to-noise ratio for the developed sensors in the presence of electromagnetic noise generated by DC motors has as high value as 52 dB . The cost of the sensor is in times cheaper than of commercially available one. In order to smooth the signal acquired from the sensors, we implemented the digital low-pass filtering technique with the cut-off frequency of 70 Hz . Specifications of the developed optical torque sensors and analogous 6-axis T/F sensors are listed in Table 3.

The main advantages of ATI sensors²⁰ are high torsional stiffness and large factor of safety. The 6-axis force/torque sensors of the Minebea Co. have small electrical noise level. However, the weight and sizes make difficulties for their application as joint torque detector in robot. Such features of newly developed optical torque sensors as high dependability, good accuracy (even in electrically noisy environment), low price, compact sizes, lightweight, easy manufacturing procedure make the developed sensors better solution comparing with analogs for the torque measurement in robot arm joints.

In addition to the contact force, torque sensor continuously measures the gravity load. To extract the value of the contact force from the sensor signal, we elaborated the gravity compensation algorithm based on Newton-Euler dynamics formulation. The plot of measured (while rotating) and calculated values of torque acting on the fourth joint is shown in Fig. 10. The plot of error of the torque measurement is presented in Fig. 11.

Table 3. Technical specification.

Sensor	First joint	Second joint	Third/ Fourth joint	ATI Mini 45SI-290-10	ATI Mini 40SI-80-4	Minebea OPFT-100N	Minebea OPFT-220N
Sensing range [\pm Nm]	12.5	10.5	4.5	10.0	4.0	5.0	11.0
Torsional stiffness [Nm/rad]	3,230	2,730	950	35,000	4,300	—	—
Factor of safety	1.76	1.7	1.82	5.4	4.3	1.5	1.5
Outer diameter [mm]	45.0	42.0	37.0	45.0	40.0	50.0	50.0
Thickness [mm]	7.0	6.0	5.0	15.7	12.25	31.5	31.5
Sensor mass [g]	70.15	50.81	34.95	92.0	50.0	330.0	330.0

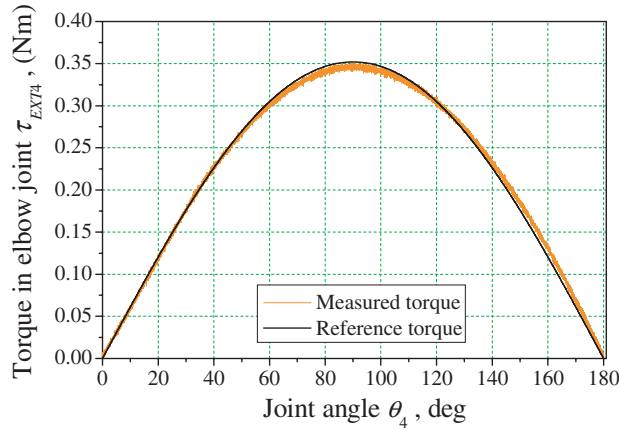


Fig. 10. Measured and referenced torques.

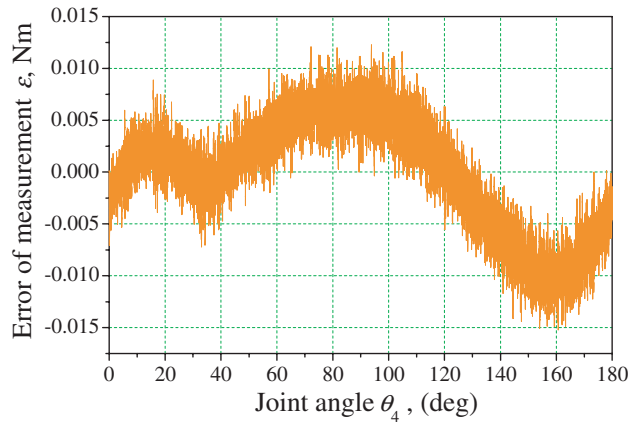


Fig. 11. Error of torque measurement.

Observing the measurement error plot, we can assign the relevant threshold of 0.015 Nm that triggers control of the constraint motion.

4. Joint Admittance Control and Joint Flexibility Consideration

4.1. Joint admittance control

People can perform dexterous contact tasks in daily activities, regulating their own dynamics according to a time-varying environment. The most efficient method of controlling the interaction between a manipulator and an environment is impedance control.²¹ This approach enables us to regulate response properties of the robot to external forces through modifying the mechanical impedance parameters. In many studies, the adaptive model-based impedance control is adopted.^{22,23} However, due

to parametric uncertainties of the robot dynamics model, it is difficult to obtain the complete description of the dynamics. Therefore, model-based adaptive impedance control must rely on either repeated motions or time for adaptation to achieve convergence to the desired system parameters. For systems with more than 1 DOF, such an approach can hardly be applied. To ensure the effectiveness of service task accomplishment, we decided to implement position-based impedance control (admittance control). In this algorithm, the compliant trajectory generated by the impedance controller is tracked by the PD control loop. The desired impedance properties of i th joint of manipulator can be expressed as:

$$J_{di}\Delta\ddot{\theta}_i + D_{di}\Delta\dot{\theta}_i + K_{di}\Delta\theta_i = \tau_{EXTi}; \quad \Delta\theta_i = \theta_{ci} - \theta_{di}, \quad (5)$$

where J_{di} , D_{di} , K_{di} are the desired inertia, damping, and stiffness of the i th joint, respectively; τ_{EXTi} is the torque applied to i th joint and caused by external forces, $\Delta\theta_i$ is the difference between the current position θ_{ci} and desired position θ_{di} . The state-space presentation of the equation of local impedance control is written as:

$$\begin{bmatrix} \Delta\dot{\theta}_i \\ \dot{v}_i \end{bmatrix} = \begin{bmatrix} 0 & 1 \\ -K_d/J_d & -D_d/J_d \end{bmatrix} \begin{bmatrix} \theta_i \\ v_i \end{bmatrix} + \begin{bmatrix} 0 \\ 1/J_d \end{bmatrix} \tau_{EXTi}(t), \quad (6)$$

or:

$$\begin{bmatrix} \Delta\dot{\theta}_i \\ \dot{v}_i \end{bmatrix} = A \begin{bmatrix} \theta_i \\ v_i \end{bmatrix} + B\tau_{EXTi}(t), \quad (7)$$

where the state variable is defined as $v_i = \Delta\dot{\theta}_i$; A , B are matrices. After integration of Eq. (7), the discrete time presentation of the impedance equation is expressed as:

$$\begin{bmatrix} \Delta\theta_{k+1} \\ \Delta\dot{\theta}_{k+1} \end{bmatrix} = A_d \begin{bmatrix} \Delta\theta_k \\ \Delta\dot{\theta}_k \end{bmatrix} + B_d T_{EXT(k)}. \quad (8)$$

To achieve the fast non-oscillatory response on the external force, we assigned the eigenvalues λ_1 and λ_2 of matrix A as real and unequal $\lambda_1 \neq \lambda_2$. By using Cayley-Hamilton method for matrix exponential determination, we have:

$$A_d = e^{AT} = \frac{1}{\lambda_1 - \lambda_2} \begin{bmatrix} e^{\lambda_2 T} \lambda_1 - e^{\lambda_1 T} \lambda_2 & e^{\lambda_1 T} - e^{\lambda_2 T} \\ -b(e^{\lambda_1 T} - e^{\lambda_2 T}) & e^{\lambda_2 T}(\lambda_1 + a) - e^{\lambda_1 T}(\lambda_2 + a) \end{bmatrix} \quad (9)$$

$$B_d = (A_d - I)A^{-1}B = -\frac{c}{b(\lambda_1 - \lambda_2)} \begin{bmatrix} e^{\lambda_2 T} \lambda_1 - e^{\lambda_1 T} \lambda_2 - (\lambda_1 - \lambda_2) \\ -b(e^{\lambda_1 T} - e^{\lambda_2 T}) \end{bmatrix}, \quad (10)$$

where T is the sampling time; coefficients a , b , and c are equal to D_d/M_d , K_d/M_d , and $1/M_d$, respectively; I is the identity matrix. The eigenvalues λ_1 and λ_2 can be calculated from:

$$\lambda_1 = \frac{-a + \sqrt{a^2 - 4b}}{2}; \quad \lambda_2 = \frac{-a - \sqrt{a^2 - 4b}}{2}. \quad (11)$$

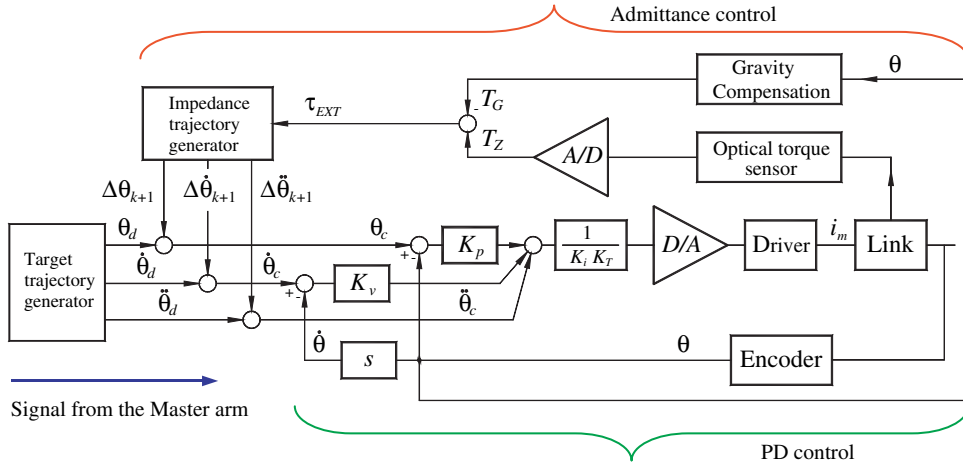


Fig. 12. Block diagram of admittance control.

We adopted $K_d = 29$ (Nm/rad), $D_d = 6.9$ (Nm·s/rad), $J_d = 0.4$ (kg·m²), to achieve closed to critical damped response and sufficient for safe interaction compliance.

To verify the theory and to evaluate the feasibility and performance of the proposed admittance controller (Fig. 12), the experiments were conducted with developed teleoperated robot arm.

During the first experiment, a person pushed the robot forearm once. The experimental results for the elbow joint — applied torque, angle generated by admittance controller, measured joint angle, and torque versus joint angle — are presented in Figs. 13–16, respectively.

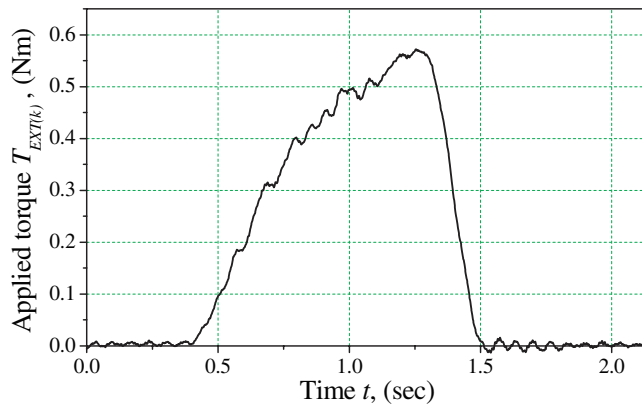


Fig. 13. External torque.

714 *D. Tsetserukou, N. Kawakami & S. Tachi*

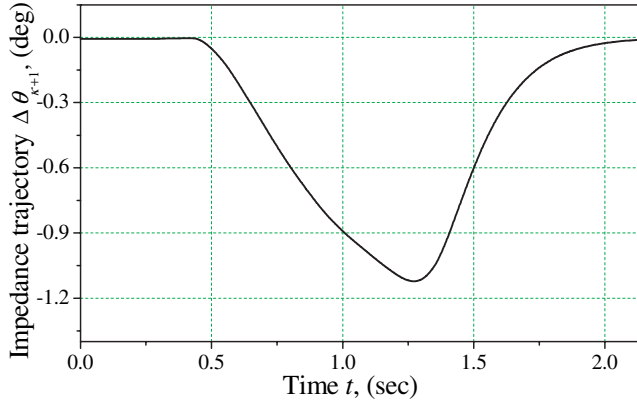


Fig. 14. Compliant trajectory.

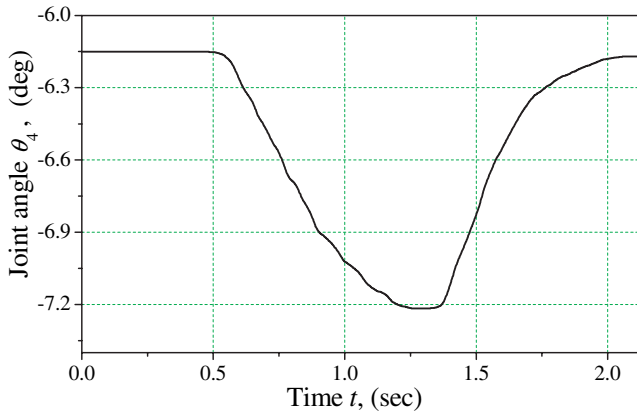


Fig. 15. Measured joint angle.

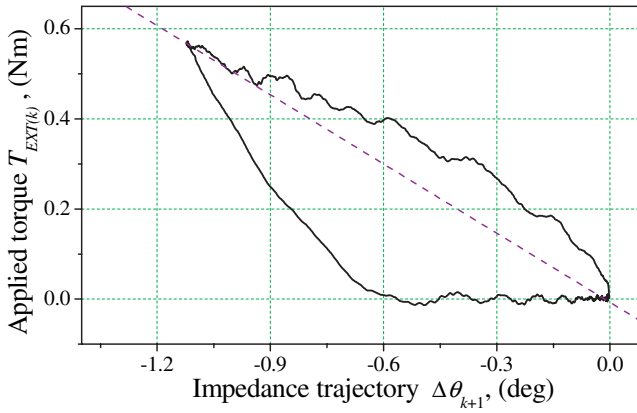


Fig. 16. Joint angle trace error.

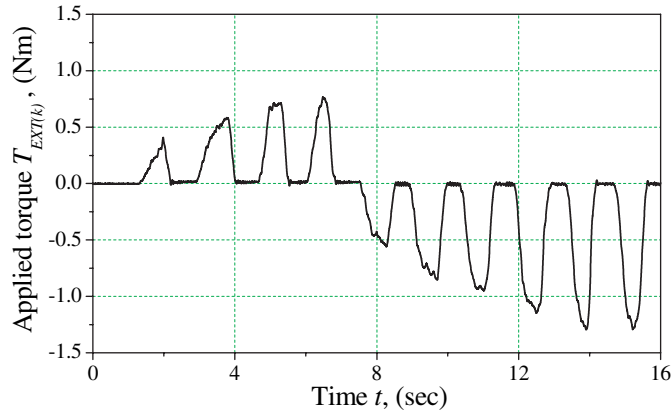


Fig. 17. External torque.

During the second experiment, a person pushed the robot forearm several times in opposite directions with forces having different magnitude. The plots of the applied torque, angle generated by admittance controller, measured joint angle, and error of joint angle in the function of time are given in Figs. 17–20, respectively.

The experimental results show the successful realization of the joint admittance control. While contacting with human, the robot arm generates compliant soft motion according to the sensed force (Figs. 14 and 18). The larger force applied to the robot arm, the more compliant trajectory is generated by impedance controller (Fig. 18). As we assigned closed to critically damped response of dynamic model to disturbance force, output angle ($\Delta\theta_{k+1}$) has ascending-descending exponential trajectory. The dash line in Fig. 16 indicates the stiffness while steady-state behavior. PD control provides small joint angle trace error in borders of -0.2° – 0.25° (Fig. 20). The conventionally force-controlled robot can provide contacting task only at the tip of the end-effector with predetermined dynamics. By contrast, our approach provides delicate and safe physical interaction of all surface of the robot arm with the environment.

In order to verify the ability of the developed robot arm to safely interact with humans and to perform cooperative tasks through the human-following motion, the experiments were conducted. The robot arm was controlled by the program on a DELL Precision computer (CPU: Intel Pentium, 3.2 GHz, memory 2 GB). Figure 21 demonstrates the physical interaction of a human with the robot forearm in the cases of the human-following motion and the haptic communication (e.g., handshaking). The robot arm generates compliant motion according to the applied force value and the desired impedance properties of the manipulator. The example of robot upper arm reaction to the force exerted by a human is presented in Fig. 22. The human operator can easily adjust the position of the robot links while teaching the robot a new motion trajectory (Fig. 23). The dynamic behavior of the robot arm

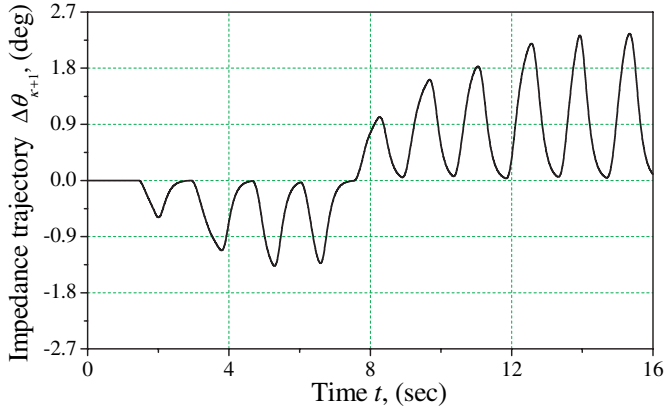


Fig. 18. Compliant trajectory.

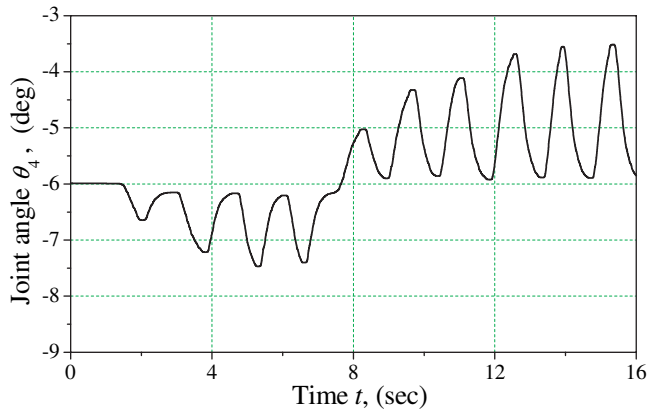


Fig. 19. Measured joint angle.

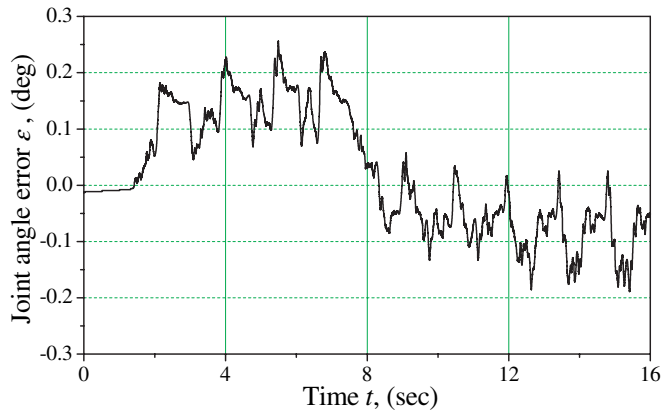


Fig. 20. Joint angle trace error.



Fig. 21. Physical interaction of a human with the robot forearm.



Fig. 22. Haptic interaction with the upper arm of robot.

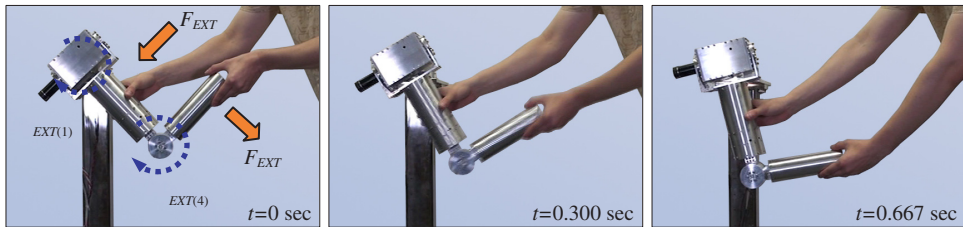


Fig. 23. Human-following motion.

colliding with human hand is shown in Fig. 24. The robot arm generates continuous compliant motion downward, thus smoothing the impact forces considerably.

It can be seen from Figs. 21–24 that the developed joint admittance controller and whole-sensitive robot arm enable the human to control the position and orientation of the robot arm, and to realize the human-following motion through haptic

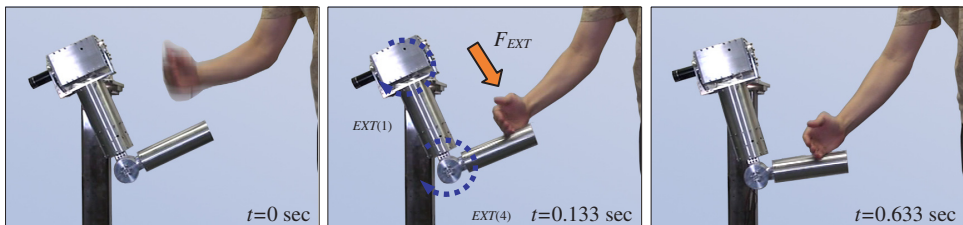


Fig. 24. Collision of a human hand and the robot forearm.

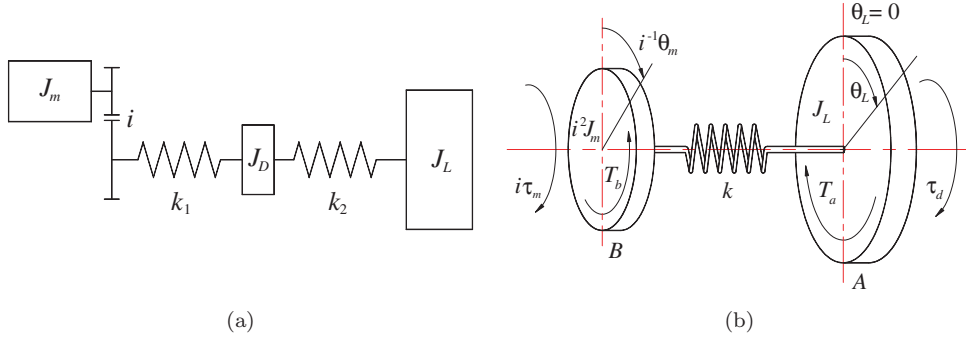


Fig. 25. Presentation of joint with flexibility.

interaction along the entire robot arm surface. The robot successfully prevents the large impact forces during the collision with a human, thus improving the safety of human-robot coexistence greatly.

4.2. Joint flexibility consideration

Flexibility introduced into robot arm joint through harmonic drive and torque sensors changes the dynamic behavior of mechanical structure. Robot joint with compliance can be represented as three-inertia system (Fig. 25(a)) including: (1) the inertias of motor J_m , harmonic drive output shaft J_D , and load J_L ; (2) the spring elements of harmonic drive (with torsional stiffness k_1) and torque sensor (with torsional stiffness k_2). Due to negligible value of inertia of output shaft of harmonic drive, three-inertia model can be reduced to the equivalent two-DOF one with mass inertias $i^2 J_m$ and J_L (Fig. 25(b)).

The torsional stiffnesses k_1 , k_2 , and equivalent spring constant k_e derived from Eq. (12) are listed in Table 4.

$$\frac{1}{k_e} = \frac{1}{k_1} + \frac{1}{k_2}, \quad k = k_e = \frac{k_1 k_2}{k_1 + k_2}. \quad (12)$$

The dynamic equations of the n -DOF manipulator with joint compliance in joint space coordinates can be obtained by D'Alembert's principle. The equations of oscillations for mass A (Eq. (13)) and mass B (Eq. (14)) ignoring damping are as follows:

$$\begin{cases} J_L(\theta_L) \ddot{\theta}_L = k (i^{-1} \theta_m - \theta_L) + \tau_d, & (13) \\ J_m \ddot{\theta}_m = -i^{-1} k (i^{-1} \theta_m - \theta_L) + \tau_m, & (14) \\ \tau_d = \tau_{EXT} - G(\theta_L) - C(\theta_L, \dot{\theta}_L) \dot{\theta}_L, & (15) \\ \tau = k (i^{-1} \theta_m - \theta_L), & (16) \end{cases}$$

where $\theta_L, \dot{\theta}_L, \ddot{\theta}_L \in R^n$ are the vectors of the link angles, the link angular velocities, and the link angle accelerations, respectively; $\theta_m, \dot{\theta}_m \in R^n$ are the vectors of motor angles, and the motor angle accelerations, respectively; $k \in R^{n \times n}$ is the diagonal

Table 4. The torsional stiffnesses of robot joints.

Parameters	Arm joints			
	Shoulder			Elbow
	J1, Pitch	J2, Roll	J3, Yaw	J4, Pitch
Torsional stiffness of harmonic drive k_1 [kNm/rad]	6.1	6.1	3.33	3.33
Torsional stiffness of the torque sensors k_2 [kNm/rad]	3.23	2.73	0.95	0.95
Equivalent torsional stiffness k_e [kNm/rad]	2.112	1.886	0.739	0.739

matrix of joint stiffness; $i \in R^n$ is the vector of gear reduction ratios; $J_L(\theta_L) \in R^{n \times n}$ is the symmetric, positive definite link inertia matrix; $J_m \in R^{n \times n}$ is the diagonal, positive definite rotor inertia matrix; $\tau_d \in R^n$ is the vector of disturbance torques; $\tau_m \in R^n$ is the vector of torques applied by motor; $\tau_{EXT} \in R^n$ is the vector of applied external joint torques; $G(\theta_L) \in R^n$ is the vector of gravitational torques; $C(\theta_L, \dot{\theta}_L) \in R^n$ represents the vector of Coriolis and centrifugal torques; $\tau_m \in R^n$ is the vector of torques applied by motor; the torque in the shaft $\tau \in R^n$ is directly proportional to twist angle $\theta = (i^{-1}\theta_m - \theta_L)$.

The transfer function from motor torque τ_m to link angle θ_L is expressed by:

$$W = \frac{\theta_L}{\tau_m} = \frac{\omega_L^2}{J_m s^2 i (s^2 + \omega_n^2)}. \quad (17)$$

The natural frequency of two-mass system ω_n and natural frequency of one-mass robot joint ω_L are derived from the following equations:

$$\omega_n = \sqrt{k \left(\frac{1}{i^2 J_m} + \frac{1}{J_L} \right)}, \quad \omega_L = \sqrt{\frac{k}{J_L}}. \quad (18)$$

The experimental results of human-robot interaction for the first joint (the most loaded one) show that despite the smooth trajectory (Fig. 26) generated by the admittance controller according to the sensed joint torque, the vibratory behavior caused by unbalanced inertial load is recorded by torque sensor (Fig. 27).

Different approaches to control the robot with flexible joints are proposed by researchers. Spong²⁴ proposed to use nonlinear control methods: (1) the feedback linearization technique and (2) the integral manifold method. Such approaches require the exact knowledge of robot arm parameters. Techniques that attenuate vibrations by using negative torque feedback were elaborated.^{25,26} The idea behind this approach is that negative torque feedback reduces the effective inertia of the motor rotor in (K_T+1) times, where K_T is the torque gain. However, whereas this approach can suppress the vibrations to some extent, it cannot control the main source of vibrations, namely, the inertial loading.

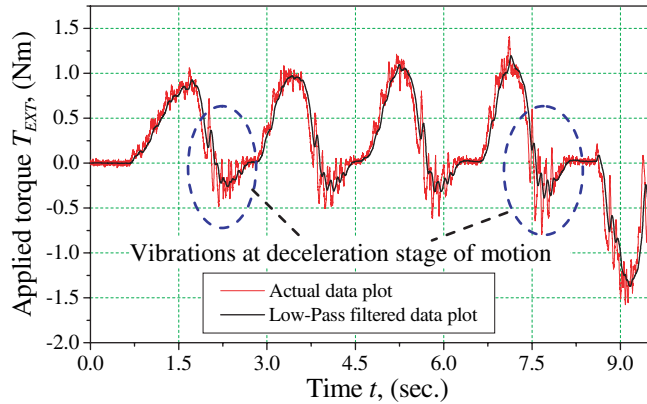


Fig. 26. External torque.

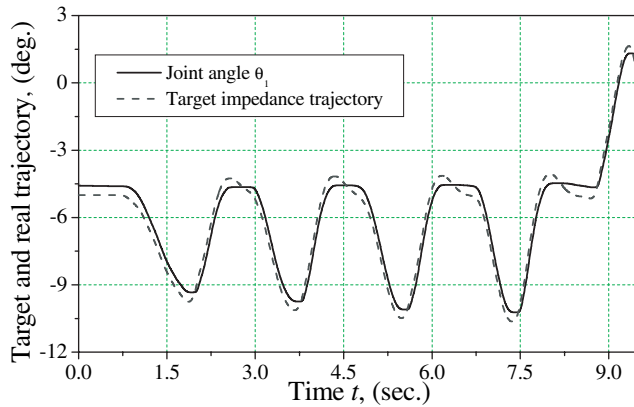


Fig. 27. Compliant trajectory and joint angle.

Through conducting the experiments we came to conclusion that there are two robust solutions. The straightforward and simple approach is to increase the coefficient of the desired damping of the heavily loaded joints. It leads to a small magnitude of the joint angle acceleration and deceleration. However, with high damping we cannot achieve a fast reaction of the robot upper arm to impact forces. The approach proposed by us is to employ position feedback based on information from accelerometer and lead controller to improve the damping property of the compliant robot joint. The angular position of the link is calculated from accelerometer data by means of double integration and high-pass filtering. The detailed procedure of oscillation parameter identification and design of vibration damping controller are given in the paper.²⁷ The block diagram of the closed loop system with lead compensator is shown in Fig. 28.

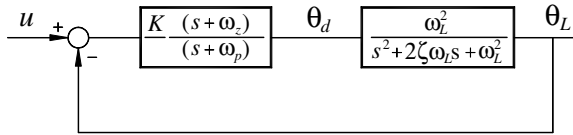


Fig. 28. System with lead compensator.

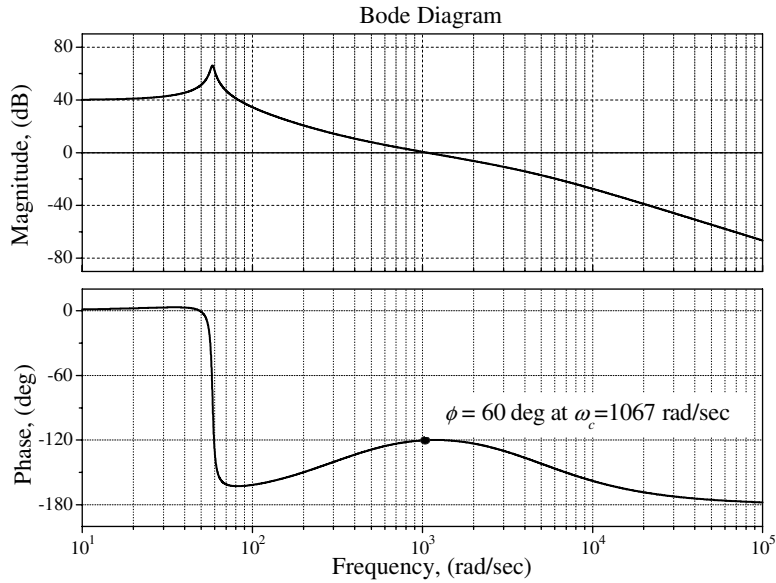


Fig. 29. Bode diagram.

The discrete presentation of the lead compensator with sampling time of T is:

$$x_{(k+1)} = e^{-\omega_p T} x_{(k)} + ((1 - e^{-\omega_p T}) / \omega_p) U_{c(k)}, \tag{19}$$

$$y_{(k)} = \theta_{d(k)} = (\omega_z - \omega_p) x_{(k)} + U_{c(k)}, \tag{20}$$

where $U_{c(k)}$ is the discrete input signal; ω_z, ω_p are the zero and pole.

The obtained value of desired load angle θ_d is then processed by PD control loop. The magnitude curve and phase-angle curve for the compensated system are shown in Fig. 29. The phase and gain margins are 60 deg. and $+\infty$, respectively. Therefore, compensated system meets both the steady-state and the relative stability requirements. Thus, the desirable transient behaviour was achieved through usage of lead compensator.

We conducted the experiment in order to evaluate the performance of the proposed damping controller. During the experiment, elbow joint was fixedly mounted, and the impulse force was applied to the tip of the robot forearm. The acceleration

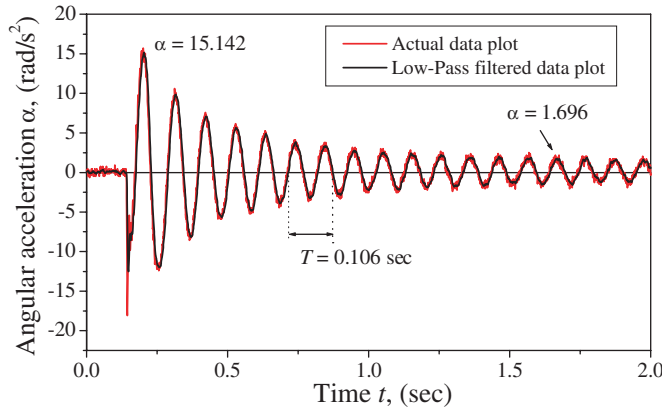


Fig. 30. Acceleration without controller.

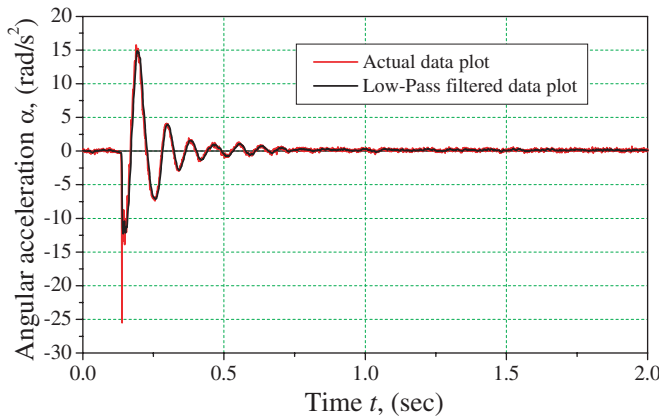


Fig. 31. Acceleration with controller.

signals without and with vibration damping controller (Figs. 30 and 31, correspondingly) were recorded. To eliminate high frequency noise, the digital low-pass filter was deployed with cut-off frequency of 100 Hz.

The experimental results show the successful damping of oscillation magnitude. The system resists the quick change in angular speed, and, therefore, provides more smooth dynamic behavior.

5. Conclusion

New whole-sensitive teleoperated robot arm iSoRA was developed to provide human-like capabilities of contact task performing in a wide variety of environments. To facilitate the developed anthropomorphic arm with joint torque measuring ability, the new optical torque sensors characterized by good accuracy, high

signal-to-noise ratio, compact sizes, easy manufacturing, high signal bandwidth, robustness, and low cost were designed and manufactured. The main novelty of our method is application of the optical approach based on the ultra-small size PI RPI-121 as sensitive element. The effectiveness of the admittance control for ensuring the safety in human-robot interaction was experimentally illustrated on a new whole-sensitive robot arm.

To compensate joint flexibility effect, we elaborated the dynamic model of the robot joint as two-mass system. The system with lead compensator and angular position of the load feedback is proposed to dump undesired vibrations. The oscillation parameters required to design the lead controller were determined by using experimental data and analytical equations. The experimental results show high performance of the developed controller in terms of successful damping of vibrations.

The developed robot iSoRA and control system have great potential to impact on the robot technologies for emerging human-robot coexistence society. In future, such robots will assist humans in daily life tasks, and provide the physical collaborative interaction and haptic communication while ensuring safety to the humans.

Acknowledgments

The research was supported in part by a Japan Society for the Promotion of Science (JSPS) Postdoctoral Fellowship for Foreign Scholars.

References

1. I. Asimov, *I, Robot*, (New York: Doubleday & Company, 1950).
2. Y. Sakagami, R. Watanabe, C. Aoyama, S. Matsunaga, N. Higaki and K. Fujimura, The intelligent ASIMO: System overview and integration, *IEEE/RSJ Int. Conf. on Intelligent Robots and Systems (IROS)* (IEEE Press, Lausanne, Switzerland, 2002), pp. 2478–2483.
3. K. Kaneko, F. Kanehiro, S. Kajita, H. Hirukawa, T. Kawasaki, M. Hirata, K. Akachi and T. Isozumi, Humanoid Robot HRP 2, in *IEEE Int. Conf. Robotics and Automation (ICRA)* (IEEE Press, New Orleans, 2004), pp. 1083–1090.
4. V. J. Lumelsky and E. Cheung, Real-time collision avoidance in teleoperated whole-sensitive robot arm manipulators, *IEEE Trans. on Systems, Man, and Cybernetics* **23**(1) (1993) 194–203.
5. N. Mitsunaga, T. Miyashita, H. Ishiguro, K. Kogure and N. Hagita. Robovie IV: A communication robot interacting with people daily in an office, *Proc. IEEE/RSJ Int. Conf. Intelligent Robots and Systems (IROS)* (IEEE Press, San Diego, US, 2006), pp. 5066–5072.
6. C. H. Wu and R. P. Paul, Manipulator compliance based on joint torque control, *Proc. IEEE Conf. Decision and Control* (IEEE Press, Albuquerque, US, 1980), pp. 88–94.
7. G. Hirzinger, A. Albu-Schaffer, M. Hahnle, I. Schaefer and N. Sporer, On a new generation of torque controlled light-weight robots, *Proc. IEEE Int. Conf. Robotics and Automation (ICRA)* (IEEE Press, Seoul, Korea, 2001), pp. 3356–3363.
8. M. Hashimoto, Y. Kiyosawa and R. P. Paul, A torque sensing technique for robots with harmonic drives, *IEEE Trans. on Robotics and Automation* **9**(1) (1993) 108–116.

9. I. Golder, M. Hashimoto, M. Horiuchi and T. Ninomiya, Performance of gain-turned harmonic drive torque sensor under load and speed conditions, *IEEE/ASME Trans. on Mechatronics* **6**(2) (2001) 155–160.
10. T. Sakaki and T. Iwakane, Impedance control of a manipulator using torque-controlled lightweight actuators, *IEEE Trans. Industry Applications* **28**(6) (1992) 1399–1405.
11. A. Bicchi and G. Tonietti, Fast and soft arm tactics: dealing with the safety-performance trade-off in robot arms design and control, *IEEE Robotics and Automation Magazine* **11**(2) (2004) 22–33.
12. S. Tachi, N. Kawakami, M. Inami and Y. Zaitso, Mutual teleexistence system using retro-reflective projection technology, *International Journal of Humanoid Robotics* **1**(1) (2004) 45–64.
13. R. Tadakuma, Y. Asahara, H. Kajimoto, N. Kawakami and S. Tachi, Development of anthropomorphic multi-D.O.F. master-slave arm for mutual teleexistence, *IEEE Trans. on Visualization and Computer Graphics* **11**(6) (2005) 626–636.
14. D. Tsetserukou, R. Tadakuma, H. Kajimoto and S. Tachi, Optical torque sensors for implementation of local impedance control of the arm of humanoid robot, *Proc. IEEE Int. Conf. Robotics and Automation (ICRA)* (IEEE Press, Orlando, US, 2006), pp. 1674–1679.
15. S. Hirose and K. Yoneda, Robotic sensors with photodetecting technology, *Proc. 20th Int. Symp. on Industrial Robots (ISIR)* (Tokyo, Japan, 1989), pp. 271–278.
16. A. Kitamura, S. Adachi and S. Tanabe, Optical displacement sensor and external force detecting device, US Patent 7 057 154 B2, Jun 6, 2006.
17. Minebea, 6-Axial Force Sensor, *Minebea Co., Ltd.*, [Online], Available: <http://www.minebea-mcd.com/6-axial/index.htm>.
18. Photointerrupter Design Guide. *Product Catalog of ROHM*, pp. 6–7, 2005.
19. D. Vischer and O. Khatib, Design and development of high-performance torque controlled joints, *IEEE Trans. on Robotic and Automation* **11**(4) (1995) 537–544.
20. ATI, Multi-axis F/T sensor, *ATI Industrial Automation*, [Online], Available: <http://www.ati-ia.com/>
21. N. Hogan, Impedance control: an approach to manipulation, Part I–III, *Trans. of ASME Journal of Dynamic Systems, Measurement and Control* **107** (1985) 1–23.
22. R. Carelli and R. Kelly, Adaptive impedance/force controller for robot manipulators, *IEEE Trans. Automatic Control* **36**(8) (1991) 967–972.
23. R. Colbaugh and A. Engelmann, Adaptive compliant motion control of manipulators: theory and experiments, *Proc. IEEE Int. Conf. on Robotics and Automation (ICRA)* (IEEE Press, San Diego, US, 1994), pp. 2719–2725.
24. M. W. Spong, Modeling and control of elastic joint robots, *Trans. of ASME Journal of Dynamic Systems, Measurement and Control* **109**(4) (1987) 310–319.
25. G. Zhang and J. Furusho, Control of robot arms using joint torque sensors, *Proc. IEEE Int. Conf. Robotics and Automation (ICRA)* (IEEE Press, Albuquerque, US, 1997), pp. 3148–3153.
26. C. Ott, A. Albu-Schaffer, A. Kugi, S. Stramigioli and G. Hirzinger, A passivity based cartesian impedance controller for flexible joint robots — Part I: Torque feedback and gravity compensation, *Proc. IEEE Int. Conf. Robotics and Automation (ICRA)* (IEEE Press, New Orleans, US, 2004), pp. 2659–2665.
27. D. Tsetserukou, N. Kawakami and S. Tachi, Vibration damping control of robot arm intended for service application in human environment, *Proc. IEEE-RAS Int. Conf. on Humanoids Robots (Humanoids)* (IEEE Press, Daejeon, Korea, 2008), pp. 441–446.



Dzmity Tsetserukou received his BS degree with honors in Electrical Engineering from the Mogilev Machine Building Institute, Belarus, in 1999, the MS degree in Mechanical Engineering from the National Academy of Sciences of Belarus, in 2002, and the PhD degree in Information Science and Technology from the University of Tokyo, Japan, in 2007. From 2002 to 2004, he was a Research Associate in the scientific research group at the National Academy of Sciences of Belarus. He is currently a JSPS Post-Doctoral Fellow in the Department of Information Physics and Computing at the University of Tokyo, Japan. He is a member of the IEEE and VRSJ and the author of over 50 technical publications, 3 patents, book chapter, and a book. His research interests include humanoid robots, force/torque sensors, impedance and admittance control, teleoperation, haptic interfaces and displays, and affective haptics.



Naoki Kawakami received his MS and PhD degrees from the University of Tokyo, Japan, in 1996 and 1999, respectively. He is currently a Lecturer in the Department of Information Physics and Computing at the University of Tokyo. His research interests include virtual reality, real-time remote robotics, telexistence, and retro-reflective projection technology. He is the author of over 150 technical publications.



Susumu Tachi received his BS, MS and PhD degrees from the University of Tokyo, in 1968, 1970 and 1973, respectively. From 1975 to 1989, he was a Director of the Biorobotics Division at the Mechanical Engineering Laboratory, Ministry of International Trade and Industry, Tsukuba Science City, Japan. From 1989 to 2009, he was a Professor in the Department of Information Physics and Computing, the University of Tokyo. He is currently a Professor in the Graduate School of Media Design, Keio University, Japan. He is a Founding Director of the Robotic Society of Japan (RSJ), and a Founding President of the Virtual Reality Society of Japan (VRSJ). From 1988, he serves as a Chairman of the IMEKO (International Measurement Confederation) Technical Committee on Measurement in Robotics. He is a member of IEEE VR Steering Committee, and he served as a General Chair of IEEE VR 2001 and 2002. He was responsible for the following research projects: Guide Dog Robot (1976–1983), National Large Scale Project on Advanced Robotics in Hazardous Environment (1983–1990), National Large Scale Project on Humanoids and Human Friendly Robotics (HRP) (1998–2003), and CREST Project on Telexistence Communication Systems (2000–2005). He is the author of over 500 technical publications. His research interests include virtual reality, real-time remote robotics, telexistence, and retro-reflective projection technology.

